

Cat-qubit-inspired gate on $\cos(2\theta)$ qubits

Catherine Leroux^{1,*} and Alexandre Blais^{1,2}

¹*Institut quantique & Département de Physique, Université de Sherbrooke, Sherbrooke J1K 2R1 QC, Canada*

²*Canadian Institute for Advanced Research, Toronto, ON, Canada*

(Dated: April 6, 2023)

For $\cos(2\theta)$ qubits based on voltage-controlled semiconductor nanowire Josephson junctions we introduce a single-qubit Z gate inspired by the noise-bias preserving gate of the Kerr-cat qubit. This scheme relies on a π rotation in phase space via a beamsplitter-like transformation between a qubit and ancilla qubit. The rotation is implemented by adiabatically changing the potential energies of the two qubits such as to preserve a double-well potential at all times. This gate constrains the dynamics in the subspace of a $\cos(2\theta)$ qubit at all times, therefore yielding high-fidelity operation while preserving the qubit's coherence. We introduce a circuit to realize this gate and support our findings with numerical simulations.

Introduction— The protection mechanism of the $\cos(2\theta)$ qubit relies on the disjoint support of the qubit's logical eigenstates [1, 2]. This protection mechanism, however, also makes transitions between the logical states necessary for gates difficult. Realizing gates on protected qubits therefore rely on breaking the symmetry of the qubit's potential wells or on the use of higher energy states. Both approaches expose the qubit to additional decay mechanisms, and often result in slow gates [3, 4]. Ideally, high-fidelity gates would maintain the qubit's double-well structure, thereby preserving its underlying protection, while also being fast.

The double-well structure of the potential energy of the $\cos(2\theta)$ qubit is reminiscent of the metapotential of the Kerr-cat qubit which encodes logical states in coherent states of opposite phases. In this qubit, those states are stabilized by opposing the Kerr nonlinearity of a Josephson junction with a two-photon pump [5, 6]. An advantage of this qubit is its exponentially long bit-flip time with the amplitude of the coherent states. Importantly, the two-photon drive in the Kerr-cat qubit not only stabilizes the qubit but is also a resource when realizing gates. Indeed, by adiabatically changing the phase of the drive, it is possible to implement a fast, high-fidelity π rotation of the cat states in phase space such that the two metapotential wells of the Kerr cat are swapped leading to the desired operation [7]. Because the logical states remain confined by the metapotential throughout the gate, bit-flip errors remain exponentially suppressed during the protocol.

Inspired by this approach, here we show how to realize a logical Z gate on a $\cos(2\theta)$ qubit based on voltage-controlled semiconductor nanowire Josephson junctions [8, 9]. This qubit is formed by a capacitively shunted flux-biased interferometer made from voltage-controlled semiconductor nanowire Josephson junctions. Crucially, as experimentally demonstrated in Ref. [8], this design allows to adiabatically shape the potential energy of the qubit between a single-well and a two-well potential by using the voltage bias.

The central idea of the gate introduced here is to ex-

plot this feature to perform an adiabatic manipulation of the energy potential of two semiconducting qubits, where one is the logical unit and the other is an ancillary qubit, such as to effectively rotate the $\cos(2\theta)$ potential in phase space resulting in a Z gate on the logical qubit. Although we focus on the semiconducting $\cos(2\theta)$ qubit, these ideas can be extended to other protected qubits having a double-well potential structure by supplementing that qubit with a second mode. As will be made clear below, this is possible as long as both modes can have their potential energies varied between $\cos(\theta)$ and $\cos(2\theta)$. Such qubits include the fluxonium [10] and other compact $\cos(2\theta)$ qubits [2, 4].

This article is organized as follows: We review the main properties of the superconductor-semiconductor $\cos(2\theta)$ qubit before introducing the concept of the gate. We then discuss a possible circuit implementation and present numerical results before concluding.

Superconductor-semiconductor $\cos(2\theta)$ qubit— A superconductor-semiconductor $\cos(2\theta)$ qubit is a capacitively shunted SQUID made of two semiconducting junctions which we take to be flux-biased at half-quantum flux, see Fig. 1 a) [8, 9]. Each junction can be biased with a gate voltage to control the junction's effective Josephson energy. The qubit is described by the approximate Hamiltonian (see appendix A for details on the derivation of this model)

$$\hat{H}_{\cos(2\theta)} \approx 4E_C \hat{n}_\theta^2 - \alpha \cos(\hat{\theta}) + \beta \cos(2\hat{\theta}), \quad (1)$$

where $\hat{\theta}$ is its phase operator with canonical number operator \hat{n}_θ , E_C is the charging energy, $\alpha = E_{J_1}^1 - E_{J_1}^2$ and $\beta = E_{J_2}^1 + E_{J_2}^2$ where $E_{J_k}^i(V_i)$ is the amplitude of the k th harmonic of the Andreev bound state energy of the i th junction gated with a voltage V_i . For conciseness, the voltage dependence is not made explicit in Eq. (1). As noted in Ref. [8], the junction asymmetry can be used to constrain the qubit to a single potential well (for $|E_{J_1}^1 - E_{J_1}^2| > |E_{J_2}^1 + E_{J_2}^2|$) or to two potential wells (for $|E_{J_1}^1 - E_{J_1}^2| < |E_{J_2}^1 + E_{J_2}^2|$), see Fig. 1 b).

Concept— Realizing a logical Z gate in a $\cos(2\theta)$ qubit

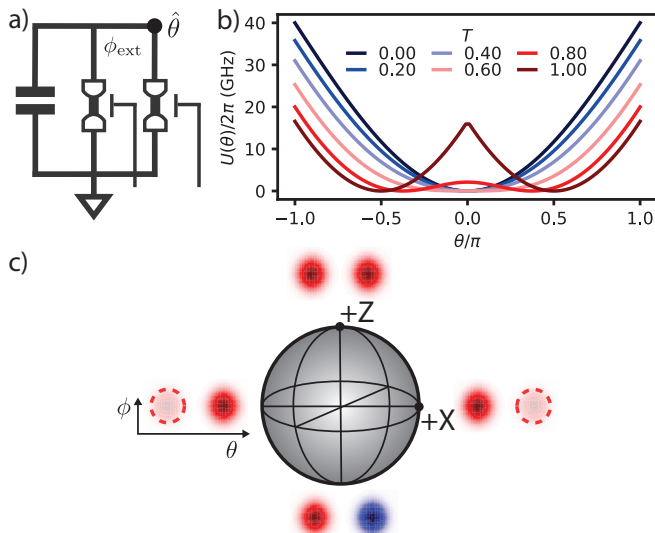


FIG. 1. a) Circuit of a superconductor-semiconductor $\cos(2\theta)$ qubit composed of two capacitively shunted semiconducting junctions in parallel, biased at half-flux quantum. b) Potential energy of the $\cos(2\theta)$ qubit assuming a single transmission channel in each of the junctions with an identical superconducting gap $\Delta/h = 40$ GHz. The transmission probability is fixed to $T = 1$ in the left junction and T is varied in the right junction. c) Bloch sphere of a logical qubit with its logical states defined and illustrated in the 2D phase space of the two qubits with phase operators θ and ϕ . Because these two operators commute, there are no interference fringes.

without breaking the qubit's protection can be challenging. Our approach to achieve this is analogous to the noise bias preserving Z gate of the Kerr-cat qubit [5] where the cat's metapotential is adiabatically rotated in phase space to perform the gate [7]. With the Kerr-cat qubit, this is realized by adiabatically changing the phase of the qubit's two-photon pump.

Inspired by this, we use a similar approach where now the control knob activating the gate is a beamsplitter angle between two modes, one having a $\cos(2\theta)$ potential and an ancilla mode with a $\cos(\phi)$ potential. As will become apparent below, the beamsplitter operation effectively swaps the double-well and single-well potential of the two modes in time, resulting in a rotation of the potential wells in the 2D plane spanned by the phase coordinates of the two modes. As in the Kerr-cat qubit, this rotation realizes a Z gate.

To better understand this dynamic, let us first consider an idealized situation starting with the Hamiltonian

$$\hat{H}_0 = 4E_{C\theta}\hat{n}_\theta^2 + \beta \cos(2\hat{\theta}) + 4E_{C\phi}\hat{n}_\phi^2 - \alpha \cos(\hat{\phi}), \quad (2)$$

describing two non-interacting modes, with the $\hat{\theta}$ mode being a $\cos(2\hat{\theta})$ qubit and the $\hat{\phi}$ mode being a transmon qubit. Here, β and α are the amplitudes of the respective potential energy, and E_{C_x} is the charging energy of the mode $x \in \{\theta, \phi\}$.

The logical states of this two-mode system are also illustrated in Fig. 1 c) in the 2D phase space of the two commuting observables $\{\hat{\theta}, \hat{\phi}\}$ with the convention that the even and odd parity states are along the Z axis. Similarly to cat qubits, the logical states are exponentially protected against Z -type errors rendering any Z gate challenging. The Z gate can, however, be robustly realized via a rotation in the 2D phase space while preserving this protection, again in analogy to the rotation in the phase space of cat qubits.

In principle, a rotation of the θ and ϕ coordinates can be implemented with the beamsplitter transformation $\hat{B}(\varphi)$ defined such that

$$\hat{B}\hat{\theta}\hat{B}^\dagger = \cos(\varphi)\hat{\theta} - \sin(\varphi)\hat{\phi}, \quad (3)$$

$$\hat{B}\hat{\phi}\hat{B}^\dagger = \cos(\varphi)\hat{\phi} + \sin(\varphi)\hat{\theta}, \quad (4)$$

where φ is the beamsplitter angle and therefore the angle of rotation of the θ and ϕ coordinates. Under this transformation the potential energy $\hat{U} = \beta \cos(2\hat{\theta}) - \alpha \cos(\hat{\phi})$ of the Hamiltonian \hat{H}_0 transforms as

$$\hat{B}\hat{U}\hat{B}^\dagger = \beta \cos\left(2[\cos(\varphi)\hat{\theta} + \sin(\varphi)\hat{\phi}]\right) - \alpha \cos\left([\cos(\varphi)\hat{\phi} - \sin(\varphi)\hat{\theta}]\right). \quad (5)$$

The rotation of the double-well potential under this transformation is illustrated in Fig. 2 a) for angles $\varphi \in [0, \pi]$. As desired, the two potential well along θ at $\varphi = 0$ exchange their place after a $\varphi = \pi$ rotation. This simple observation suggests that a Z gate can be realized by adiabatically rotating the potential energy, if implementing Eq. (5) was possible.

Since a transformation of the form of Eq. (5) appears to be difficult in practice, as an alternative we propose to approximate this operation by relying on a tunable potential energy of the form

$$\hat{U}_\varphi = \beta \cos^2(\varphi) \cos(2\hat{\theta}) - \alpha \cos^2(\varphi) \cos(\hat{\phi}) + \beta \sin^2(\varphi) \cos(2\hat{\phi}) - \alpha \sin^2(\varphi) \sin(\hat{\theta}) - \frac{\zeta}{2} \sin(2\varphi) \sin(\hat{\theta}) \sin(\hat{\phi}), \quad (6)$$

which we will show can be engineered. In this expression, ζ is the interaction strength between the two qubits, to be optimized and whose sign controls the direction of the rotation. The term proportional to ζ in Eq. (6) breaks the fourfold degeneracy of the potential of Eq. (2) such as to preserve a double-well structure at all times.

The corresponding rotation of the θ and ϕ coordinates is illustrated in Fig. 2 b) for different angles φ . We observe that Eq. (6) yields the desired rotation similar to Eq. (5) but on a square instead of a circle in the 2D phase space.

Just as in the previous example, the potential wells along θ are exchanged under this operation suggesting

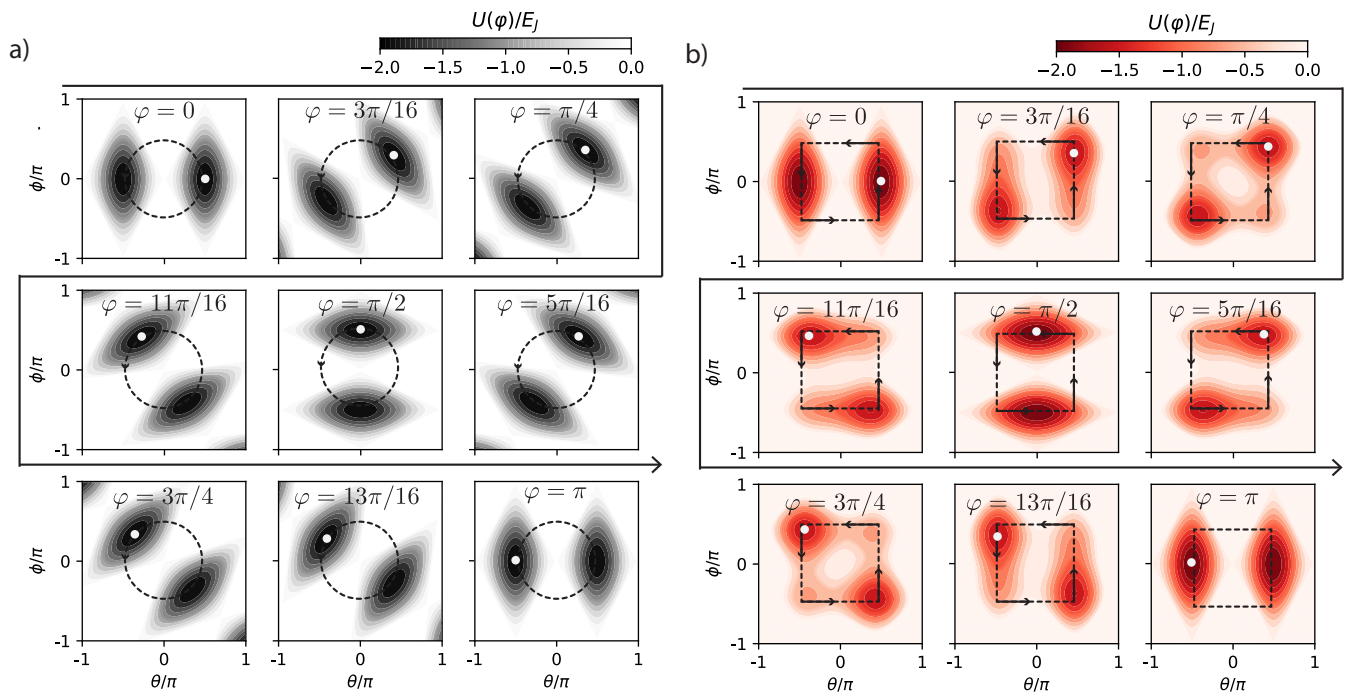


FIG. 2. a) Rotation of the potential landscape in the 2D phase space defined by the two phase coordinates θ and ϕ , obtained from the beamsplitter operation of Eq. (5). The white dot tracks the rotation of one of the two potential wells. b) Rotation resulting from the protocol in Eq. (6). This relies on the implementation of a large $\sin(\hat{\theta})\sin(\hat{\phi})$. Here $\beta = \alpha = \zeta = E_J$ for simplicity and the angles are, following the black arrow, $\varphi = 0, 3\pi/16, \pi/4, 5\pi/16, \pi/2, 11\pi/16, 3\pi/4, 13\pi/16$ and π . In b) the wells follow a square-like path instead of a circular path as in a). The θ mode, initially in a double-well potential, slowly goes through a single well potential and then back to a double-well potential while the ϕ mode does the opposite.

that a Z gate can be realized by adiabatically swapping the roles of the θ and ϕ modes, i.e. by slowly going back and forth between a double-well potential and a single well potential in each mode. The interaction ζ is used here to control the direction of the rotation. In contrast to the Kerr-cat qubit [5] where the wells move along a circle, here the wells approximately move along the edges of a square, see Fig. 2 b). As a consequence, the distance d between the two global minimum increases during the rotation, i.e. $d = \pi|\sec(\min(\varphi, \pi/2 - \varphi))|$ varies between π and $\sqrt{2}\pi$ (with $0 \leq \varphi \leq \pi/2$). This small change in the distance between the potential wells has little effect on the qubit's protection.

Below, we show how realize this concept by exploiting the fact that the superconductor-semiconductor qubit of Fig. 1 a) can be continuously tuned from having a $\cos(2\theta)$ potential to a $\cos(\theta)$ qubit by varying the transmission probability in one of its two junctions [8].

Circuit implementation— The adiabatic change between a double-well potential and a single-well potential corresponding to the first two lines of Eq. (6) can be readily realized by tuning the gate voltages at the junctions of the superconductor-semiconductor $\cos(2\theta)$ qubits such as to vary the asymmetry between the energies of the junctions. The main challenge is implementing the ideally large $\sin(\hat{\theta})\sin(\hat{\phi})$ interaction that varies in time corre-

sponding to the last line of Eq. (6). Here, we propose to use another superconductor-semiconductor interferometer, with small transmission junctions and flux-biased at half quantum flux, as a coupler implementing an interaction of the type $\cos(\hat{\theta} - \hat{\phi})$ with an amplitude ζ controlled by the asymmetry between the interferometer's two junctions, see Fig. 3 a) and appendix C for details of the derivation. Expanding the above cosine term, this approach yields both the desired $\sin(\hat{\theta})\sin(\hat{\phi})$ contribution as well as an additional error term $\cos(\hat{\theta})\cos(\hat{\phi})$. The impact of this error term is analyzed further below.

The circuit of Fig. 3 a), where the circuits of the two $\cos(2\theta)$ qubits are assumed here to be identical for simplicity, is described by the Hamiltonian

$$\begin{aligned} \hat{H} = & 4E_C\hat{n}_\theta^2 + \beta\cos^2(\varphi)\cos(2\hat{\theta}) - \alpha\sin^2(\varphi)\cos(\hat{\theta}) \\ & + 4E_C\hat{n}_\phi^2 - \alpha\cos^2(\varphi)\cos(\hat{\phi}) + \beta\sin^2(\varphi)\cos(2\hat{\phi}) \quad (7) \\ & - \frac{\zeta}{2}\sin(2\varphi)\cos(\hat{\theta} - \hat{\phi}), \end{aligned}$$

where $\alpha\sin^2(\varphi)$ and $\alpha\cos^2(\varphi)$ are the amplitudes of the first harmonic of the potential energy at an angle φ controlled by the voltage bias for modes θ and ϕ , respectively, while $\beta\cos^2(\varphi)$ and $\beta\sin^2(\varphi)$ are the amplitudes of the second harmonic, and ζ is the interaction strength. We take both modes to have charging energy E_C . We

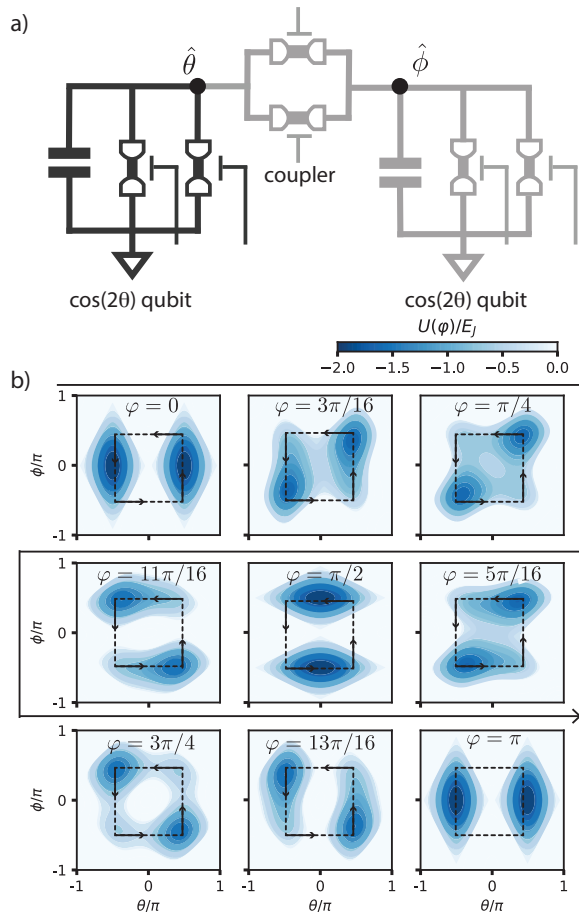


FIG. 3. a) Possible circuit realization for a noise-preserving logical Z gate in a superconductor-semiconductor $\cos(2\theta)$ qubit (in black). The coupler is used to implement a voltage-tunable $\cos(\hat{\theta} - \hat{\phi})$ interaction with the goal of approximately replicating Fig. 2 b) at low energies. b) Potential energy of Eq. (7), the Hamiltonian of the circuit in panel a), at $\varphi = 0, 3\pi/16, \pi/4, 5\pi/16, \pi/2, 11\pi/16, 3\pi/4, 13\pi/16$ and π in Eq. (6).

however note that the charging energies and the amplitudes of the first and second harmonics of the Andreev bound state energy do not need to be strictly the same for both junctions. The potential energy landscape of Eq. (7) illustrated in Fig. 3 b) approximately reproduces Fig. 2 b) preserving its essential features. In particular, we note that the total parity of the two modes θ and ϕ , $(\theta, \phi) \rightarrow (-\theta, -\phi)$, is a symmetry of the Hamiltonian in Eq. (7) for all angles φ .

Importantly, we find that the instantaneous Hamiltonian corresponding to a value of φ can be approximated at low energies by the effective model (see appendix D)

$$\hat{H} \approx 4E_C \hat{n}_\Theta^2 + \beta \cos(2\pi \hat{\Theta}/d) + 4E_C \hat{n}_\Phi^2 - \alpha \cos(d\hat{\Phi}/\pi), \quad (8)$$

where $\hat{\Theta} = \cos(\varphi)\hat{\theta} + \sin(\varphi)\hat{\phi}$ is defined along the radius of the rotation, $\hat{\Phi} = \cos(\varphi)\hat{\phi} - \sin(\varphi)\hat{\theta}$ is its perpendicular coordinate, and $d(\varphi) = \pi |\sec(\min(\varphi, |\pi/2 - \varphi|, |\pi - \varphi|))|$ is

the instantaneous distance between the two global minima. Here, the logical states are constrained to a double-well potential at all times during the Z gate with $\hat{\Theta}$ being the logical mode. As before, we note that the main consequence of following a square path instead of a circular path in the 2D phase space is the renormalization of the distance between the global potential minima which results in a small renormalization of the qubit frequency as well as the matrix elements of the noise operators.

Going back to the full model of Eq. (7), the first 6 energy levels versus φ are illustrated in Fig. 4 a) [top panel] as well as the 0-1 transition frequency [bottom panel] for $E_C/h = 100$ MHz and $\alpha/h = \beta/h = \zeta/h = 20$ GHz. The eigenstates of even parity (for conciseness) are shown in panel b) for different values of φ . We observe that the two-fold degeneracy of the spectrum is conserved for all angles φ , indicating that a $\cos(2\theta)$ potential is equally preserved. The instantaneous eigenstates of Eq. (7) are also compared against those of the ideal case where $\cos(\hat{\theta} - \hat{\phi})$ is replaced by the ideal interaction $\sin(\hat{\theta}) \sin(\hat{\phi})$ for different angles φ in appendix E. As observed in Fig. 2 b) and Fig. 3 b), both models conserve the desired double-well potential structure responsible for the protection mechanisms of the $\cos(2\hat{\theta})$ qubit.

A realistic circuit would also be subjected to external charge and flux noise (see appendix C). To leading order, the relevant noise operators are the charge operator as well as the cosine and sine phase operators of each mode. In particular, we observe that both the matrix elements of the charge operators and cosine phase operators remain exponentially suppressed during the gate's adiabatic evolution as expected from preserving a double-well structure in the total potential at all times, see Fig. 5. Similarly, the sine phase operators remain similar to logical X operators at all times. As a result, dephasing from charge noise, coming from either charge operators or cosine terms due to the voltage tunability of the junctions, is exponentially suppressed. As already noted in Ref. [11], the matrix element of the sine terms resulting from low-frequency flux noise are the main source of error for the $\cos(2\theta)$ qubit, see Fig. 5 c). These correspond to X -type errors. Importantly and in analogy to the noise-bias preserving rotation in cat qubits [7], the adiabatic evolution does not yield Z -type errors.

Numerical results for the Z gate— In what follows, we account for the time dependence in the angle $\varphi \rightarrow \varphi(t)$ with the boundary conditions $\varphi(0) = 0$ and $\varphi(T) = \pi$ such as to implement a logical Z gate where the two potential wells in the θ mode are effectively swapped at time $t = T$. As discussed in appendix F, constraints on $\varphi(t)$ can be derived from the adiabatic theorem [12] and used to optimize both the gate time and fidelity.

In absence of decoherence, we numerically simulate evolution under the Hamiltonian of Eq. (7) and find that it is possible to realize a Z gate in less than 100 ns gate with an average gate fidelity [13] above

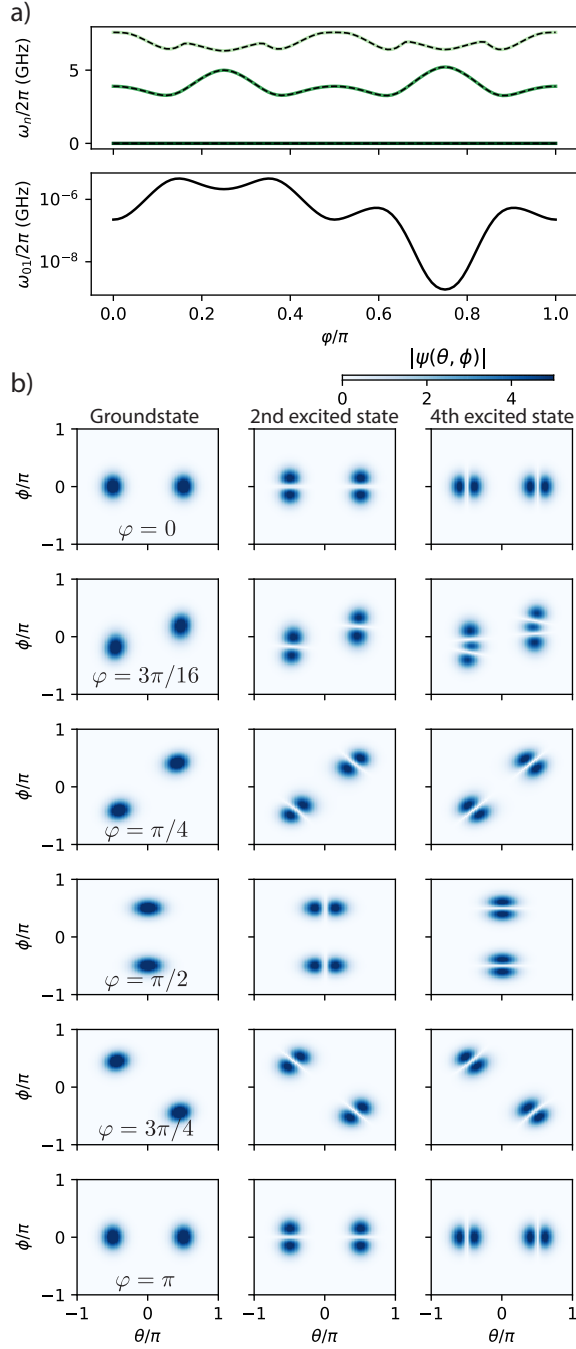


FIG. 4. a) Energy spectrum of Eq. (7), where ω_n is the n th eigenvalue, as a function of φ/π for $E_C/h = 0.1$ GHz and $\alpha/h = \beta/h = \zeta/h = 20.0$ GHz. Top panel: the n th green line corresponds to the eigenvalue ω_{2n} and the black line on top identifies the eigenvalue ω_{2n+1} . Bottom panel: qubit 0-1 transition frequency in log scale. b) Eigenstates of Eq. (7) for different angles φ . Each column corresponds to an eigenstate and each row is associated with a specific φ as identified in the left column. Each panel shows the eigenstate in phase space as a function of θ/π and ϕ/π .

99.96%, see Fig. 6 a). The fidelity is computed between the target Z gate unitary and the propagator

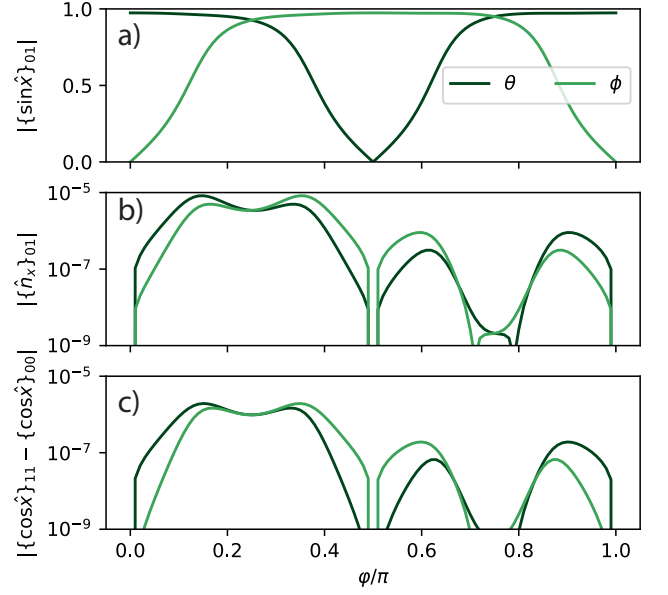


FIG. 5. a) 0 – 1 matrix elements of the sine operators resulting from flux offsets in the interferometers and resulting in bit-flips. b) 0 – 1 matrix elements of the charge operators responsible for bit-flips in presence of low-frequency charge noise. c) Frequency shifts resulting from either frequency flux noise or charge noise in the junction transparency yielding cosine terms.

$\hat{\mathcal{P}} \cdot \mathcal{T} \exp \left(-i \int_0^t d\tau \hat{H}[\varphi(\tau)] \right) \cdot \hat{\mathcal{P}}^\dagger$, where $\hat{\mathcal{P}}$ is the projector onto the logical subspace and \hat{H} is defined in Eq. (7). The shape of $\varphi(t)$ was optimized to reduce leakage during the adiabatic process (see appendix F). An example of $\varphi(t)$ is shown in Fig. 6 b) with a time evolution of initial even (first row) and odd (second row) Z states illustrated in c) resulting in a 59 ns gate with 99.97% fidelity. The methods used for the numerical simulations are detailed in appendix F. Optimal control techniques can be used to further improve the fidelity.

The limitation on the gate fidelity is better appreciated by considering the non-adiabatic correction [12] (see appendix F) which is approximately proportional to the time derivative of the effective low-energy model in Eq. (8)

$$\frac{d\hat{H}}{dt} \approx -\dot{\varphi}\beta \left(2\pi\hat{\Phi}/d \right) \sin(2\pi\hat{\Theta}/d) - \dot{\varphi}\alpha(d\hat{\Theta}/\pi) \sin(d\hat{\Phi}/\pi), \quad (9)$$

where we assumed the time-derivative of d to be negligible. The fidelity of the gate is maximized when the matrix elements $d\hat{H}/dt$ involving the instantaneous logical states are small relative to the instantaneous transition frequencies. In the small impedance limit $E_C/\alpha, E_C/\beta \ll 1$, the main source of error takes the form of a beamsplitter interaction between the two modes Θ and Φ and can be reduced by increasing the detuning

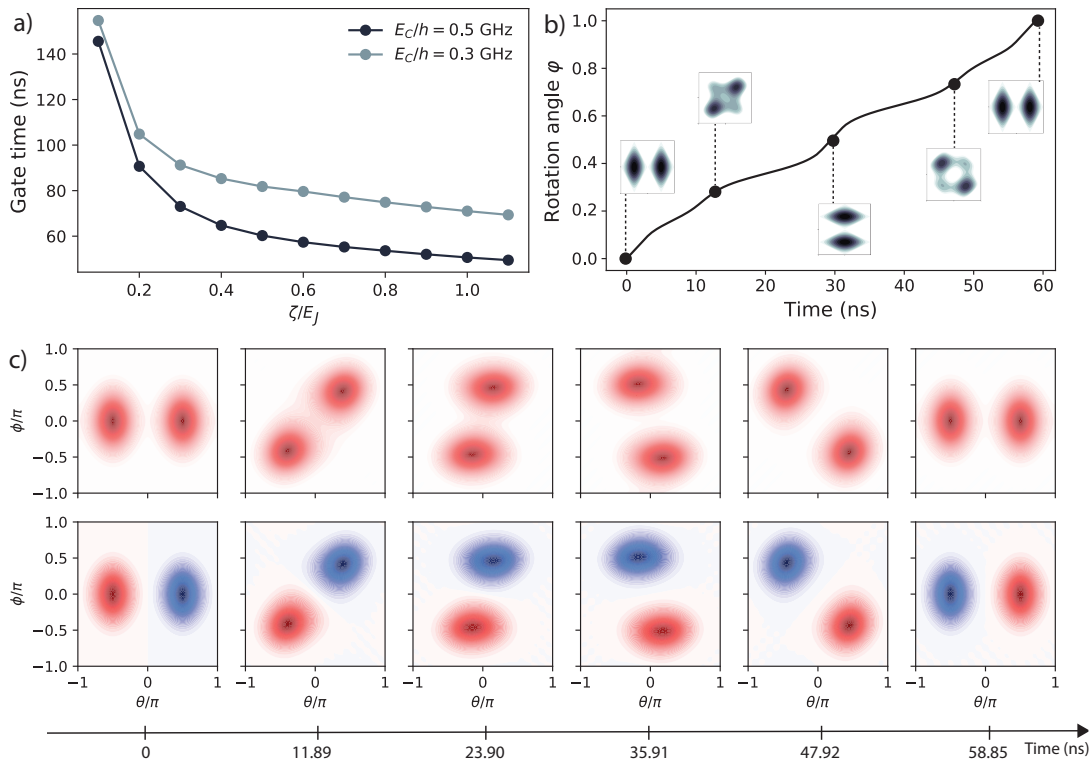


FIG. 6. a) Gate time as a function of ζ/E_J (see Eq. (7) for definitions) with $E_J/h = \alpha/h = \beta/h = 20$ GHz for two different values of the charging energy E_C . The fidelity is above 99.95% for all points. b) Example of an optimized time-dependent rotation angle $\varphi(t)$ yielding a 59 ns gate with 99.97% fidelity for $E_C/h = 0.4$ GHz. The potential energy in 2D phase space for specific times (black dots) are also shown. Details of the pulse optimization can be found in appendix F. c) Time-evolution of the even (first row) and odd (second row) Z states in the 2D phase basis with the optimized pulse in b). The time-evolution is performed using the charge basis (see appendix F for details).

between $\omega_{02}^{\Theta}(\varphi)$ and $\omega_{01}^{\Phi}(\varphi)$, where $\omega_{0n}^X(\varphi)$ is the instantaneous n th energy level of mode X at angle φ . Further optimization of the circuit parameters is left for future work.

Conclusion— We have introduced an approach to realize a protected gate on a $\cos(2\theta)$ qubit by coupling it to a second $\cos(2\theta)$ qubit such as to simultaneously preserve the protection mechanisms and realize fast high-fidelity gates. The ancillary mode allows for an effective beamsplitter operation to take place and a Z gate is realized by adiabatic manipulation of the potential energies of the two qubits, an approach which takes inspiration from gates in the Kerr-cat qubit. The scheme proposed here could in principle be realized with any protected qubit having a double-well potential by supplementing with a second mode. A gate protocol such as the one proposed here could render control in protected qubits more accessible.

ACKNOWLEDGMENTS

We are grateful to Andras Gyenis, Simon Lieu and Ross Shillito for fruitful discussions and feedback on

the manuscript. This research was funded in part by NSERC, the Ministère de l'Économie, de l'Innovation et de l'Énergie du Québec, the Canada First Research Excellence Fund, and the U.S. Army Research Office grant No. W911NF2210042.

* Catherine.Leroux@USherbrooke.ca; This work was done prior to joining AWS.

- [1] András Gyenis, Agustin Di Paolo, Jens Koch, Alexandre Blais, Andrew A. Houck, and David I. Schuster, “Moving beyond the transmon: Noise-protected superconducting quantum circuits,” *PRX Quantum* **2**, 030101 (2021).
- [2] W. C. Smith, A. Kou, X. Xiao, U. Vool, and M. H. Devoret, “Superconducting circuit protected by two-cooper-pair tunneling,” *npj Quantum Information* **6**, 8 (2020).
- [3] András Gyenis, Pranav S. Mundada, Agustin Di Paolo, Thomas M. Hazard, Xinyuan You, David I. Schuster, Jens Koch, Alexandre Blais, and Andrew A. Houck, “Experimental realization of a protected superconducting circuit derived from the $0-\pi$ qubit,” *PRX Quantum* **2**, 010339 (2021).
- [4] Agustin Di Paolo, Arne L Grimsmo, Peter Groszkowski, Jens Koch, and Alexandre Blais, “Control and coherence time enhancement of the $0-\pi$ qubit,” *New Journal of*

- Physics **21**, 043002 (2019).
- [5] Shruti Puri, Samuel Boutin, and Alexandre Blais, “Engineering the quantum states of light in a kerr-nonlinear resonator by two-photon driving,” *npj Quantum Information* **3**, 18 (2017).
- [6] A. Grimm, N. E. Frattini, S. Puri, S. O. Mundhada, S. Touzard, M. Mirrahimi, S. M. Girvin, S. Shankar, and M. H. Devoret, “Stabilization and operation of a kerr-cat qubit,” *Nature* **584**, 205–209 (2020).
- [7] Shruti Puri, Lucas St-Jean, Jonathan Gross, Alexander Grimm, Nicholas Frattini, Pavithran Iyer, Anirudh Krishna, Steven Touzard, Liang Jiang, Alexandre Blais, Steven Flammia, and Steven Girvin, “Bias-preserving gates with stabilized cat qubits,” *Science Advances* **6**, eaay5901 (2020).
- [8] T. W. Larsen, M. E. Gershenson, L. Casparis, A. Kringhøj, N. J. Pearson, R. P. G. McNeil, F. Kuemmeth, P. Krogstrup, K. D. Petersson, and C. M. Marcus, “Parity-protected superconductor-semiconductor qubit,” *Phys. Rev. Lett.* **125**, 056801 (2020).
- [9] Constantin Schrade, Charles M. Marcus, and Andrés Gyenis, “Protected hybrid superconducting qubit in an array of gate-tunable josephson interferometers,” *PRX Quantum* **3**, 030303 (2022).
- [10] Vladimir E. Manucharyan, Jens Koch, Leonid I. Glazman, and Michel H. Devoret, “Fluxonium: Single cooper-pair circuit free of charge offsets,” *Science* **326**, 113–116 (2009).
- [11] T. W. Larsen, K. D. Petersson, F. Kuemmeth, T. S. Jespersen, P. Krogstrup, J. Nygård, and C. M. Marcus, “Semiconductor-nanowire-based superconducting qubit,” *Phys. Rev. Lett.* **115**, 127001 (2015).
- [12] M V Berry, “Transitionless quantum driving,” *Journal of Physics A: Mathematical and Theoretical* **42**, 365303 (2009).
- [13] Michael A Nielsen, “A simple formula for the average gate fidelity of a quantum dynamical operation,” *Physics Letters A* **303**, 249–252 (2002).
- [14] Steven J. Weber, “Gatemons get serious,” *Nature Nanotechnology* **13**, 877–878 (2018).
- [15] A. Kringhøj, L. Casparis, M. Hell, T. W. Larsen, F. Kuemmeth, M. Leijnse, K. Flensberg, P. Krogstrup, J. Nygård, K. D. Petersson, and C. M. Marcus, “Anharmonicity of a superconducting qubit with a few-mode josephson junction,” *Phys. Rev. B* **97**, 060508 (2018).
- [16] L. Casparis, N. J. Pearson, A. Kringhøj, T. W. Larsen, F. Kuemmeth, J. Nygaard, P. Krogstrup, K. D. Petersson, and C. M. Marcus, “Voltage-controlled superconducting quantum bus,” *Phys. Rev. B* **99**, 085434 (2019).
- [17] Folkert K. de Vries, Elías Portolés, Giulia Zheng, Takashi Taniguchi, Kenji Watanabe, Thomas Ihn, Klaus Ensslin, and Peter Rickhaus, “Gate-defined josephson junctions in magic-angle twisted bilayer graphene,” *Nature Nanotechnology* **16**, 760–763 (2021).
- [18] Gil-Ho Lee, Sol Kim, Seung-Hoon Jhi, and Hu-Jong Lee, “Ultimately short ballistic vertical graphene josephson junctions,” *Nature Communications* **6**, 6181 (2015).
- [19] Mohammad T. Haque, Marco Will, Matti Tomi, Preeti Pandey, Manohar Kumar, Felix Schmidt, Kenji Watanabe, Takashi Taniguchi, Romain Danneau, Gary Steele, and Pertti Hakonen, “Critical current fluctuations in graphene josephson junctions,” *Scientific Reports* **11**, 19900 (2021).
- [20] Catherine Leroux, Adrian Parra-Rodriguez, Ross Shillito, Agustin Di Paolo, William D. Oliver, Charles M. Marcus, Morten Kjaergaard, Andrés Gyenis, and Alexandre Blais, “Nonreciprocal devices based on voltage-tunable junctions,” (2022).

Appendix A: $\cos(2\theta)$ qubit

The Andreev bound state (ABS) energy of a single superconducting-semiconducting junction (e.g. a nanowire junction) is [8, 9, 11, 14–20]

$$\varepsilon(V, \hat{\theta}) = -\Delta \sum_j \sqrt{1 - T_j(V) \sin^2(\hat{\theta}/2)}, \quad (\text{A1})$$

where Δ is the superconducting gap, $T_j(V)$ is the transmission probability of the j th channel at the gate voltage V , and $\hat{\theta}$ is the phase across the junction. Equation (A1) can be expanded in $\hat{\theta}$ harmonics as

$$\varepsilon(V, \hat{\theta}) = - \sum_{m=1}^{\infty} (-1)^{m-1} E_{Jm}(V) \cos(m\hat{\theta}), \quad (\text{A2})$$

where we have defined the positive-defined energies

$$E_{Jm}(V) = \Delta \sum_{n=m}^{\infty} 2 \binom{1/2}{n} \binom{2n}{n-m} \sum_i \frac{(-1)^{n+1} T_i^n(V)}{4^n}. \quad (\text{A3})$$

To simplify the presentation, the derivation of Eq. (A2) is presented in appendix B.

Using the above result, the Hamiltonian of the circuit of Fig. 1 a) which contains two semiconducting junctions reads

$$\hat{H}_{\cos(2\theta)} \approx 4E_C \hat{n}_\theta^2 - \alpha(V_1, V_2, \phi_{\text{ex}}) \cos(\hat{\theta}) + \beta(V_1, V_2, \phi_{\text{ex}}) \cos(2\hat{\theta}) + \epsilon(V_1, V_2, \phi_{\text{ex}}) \sin(\hat{\theta}), \quad (\text{A4})$$

where $\hat{\theta}$ is the phase operator, \hat{n}_θ the number operator and E_C the charging energy. The amplitudes of the potential energy terms take the form

$$\alpha(V_1, V_2, \phi_{\text{ex}}) = E_{J1}^1(V_1) + E_{J1}^2(V_2) \cos(\phi_{\text{ex}}) \quad (\text{A5})$$

$$\beta(V_1, V_2, \phi_{\text{ex}}) = E_{J2}^1(V_1) + E_{J2}^2(V_2) \cos(2\phi_{\text{ex}}) \quad (\text{A6})$$

$$\epsilon(V_1, V_2, \phi_{\text{ex}}) = E_{J2}^2(V_2) \sin(\phi_{\text{ex}}), \quad (\text{A7})$$

where $E_{Jk}^i(V_i)$ is the amplitude of the k th harmonic of the Andreev bound state energy of the i th junction gated with a voltage V_i , and ϕ_{ex} is the external flux bias.

Away from the flux sweet spot $\phi_{\text{ex}} = \pi$, the two potential wells become asymmetric due to the $\sin(\theta)$ term. For the remaining of this work we focus on the case $\phi_{\text{ex}} = \pi$ to simplify the discussion. We note, however, that ϵ can be tuned to implement Z gates and to facilitate state preparation in the desired potential well.

Appendix B: Expansion of the ABS energy

Taylor expanding Eq. (A1) in the transmission probabilities $T_i(V)$ yields

$$\varepsilon(V, \hat{\theta}) = -\Delta \sum_i \sum_{n=0}^{\infty} \binom{1/2}{n} (-1)^n T_i^n(V) \sin^{2n}(\hat{\theta}/2). \quad (\text{B1})$$

This expression can be put in a more useful form by using the binomial expansion of $4^n \sin^{2n} \theta = (-1)^n (e^{i\hat{\theta}} - e^{-i\hat{\theta}})^{2n}$,

$$4^n \sin^{2n}(\hat{\theta}/2) = \sum_{m=0}^{2n} \binom{2n}{m} (-1)^{n+m} e^{i(2n-m)\hat{\theta}} e^{-im\hat{\theta}} = \binom{2n}{n} + 2 \sum_{m=1}^n \binom{2n}{n-m} (-1)^m \cos(m\hat{\theta}), \quad (\text{B2})$$

where we used the change of variables $m \rightarrow n - m$. Ignoring the constant offset, we find that

$$\varepsilon(V, \hat{\theta}) = -\Delta \sum_i \sum_{n=0}^{\infty} \sum_{m=1}^n (-1)^{n+m} 2 \binom{1/2}{n} \binom{2n}{n-m} \frac{T_i^n(V)}{4^n} \cos(m\hat{\theta}), \quad (\text{B3})$$

which we can reorder as

$$\varepsilon(V, \hat{\theta}) = -\Delta \sum_i \sum_{m=1}^{\infty} \sum_{n=m}^{\infty} (-1)^{n+m} 2 \binom{1/2}{n} \binom{2n}{n-m} \frac{T_i^n(V)}{4^n} \cos(m\hat{\theta}) \quad (\text{B4})$$

to recover Eq. (A2).

Appendix C: Circuit implementation

The total Hamiltonian of the circuit in Fig. 3 a) has the form $\hat{H} = \hat{H}_\theta + \hat{H}_\phi + \hat{H}_{\theta-\phi}$ where

$$\hat{H}_x = 4E_{Cx}(\hat{n}_x - n_{\text{ex},x})^2 - \alpha_x(V_{1x}, V_{2x}, \phi_{\text{ex},x}) \cos(\hat{x}) + \beta_x(V_{1x}, V_{2x}, \phi_{\text{ex},x}) \cos(2\hat{x}) + \epsilon_x(V_{1x}, V_{2x}, \phi_{\text{ex},x}) \sin(\hat{x}) \quad (\text{C1})$$

is the $\cos(2\theta)$ qubit Hamiltonian for mode $x \in \{\theta, \phi\}$ and where we have used the results of appendices A and B. Moreover, the last term of \hat{H} takes the form

$$\hat{H}_{\theta-\phi} = g\hat{n}_\theta\hat{n}_\phi - \alpha_g(V_{1g}, V_{2g}, \phi_{\text{ex},g}) \cos(\hat{\theta} - \hat{\phi}) + \beta_g(V_{1g}, V_{2g}, \phi_{\text{ex},g}) \cos(2\hat{\theta} - 2\hat{\phi}) + \epsilon_g(V_{1g}, V_{2g}, \phi_{\text{ex},g}) \sin(\hat{\theta} - \hat{\phi}), \quad (\text{C2})$$

This represents the Hamiltonian of the coupler which is also a semiconductor interferometer mediating a capacitive coupling g between the two $\cos(2\theta)$ qubits as well as an inductive interaction through the semiconductor junctions. Here we consider $\phi_{\text{ex},x} = \pi$ for $x \in \{\theta, \phi, g\}$, the small transmission limit where $\beta_g \rightarrow 0$, and the weak coupling limit $g \rightarrow 0$. Controlling V_{1x} and V_{2x} allows us to implement the Hamiltonian in Eq. (7).

Appendix D: Low energy model

The global two-fold degenerate minima of the potential energy of Eq. (7) are approximately defined on opposite points on the edges of a square of width π

$$(\theta, \phi) = \pm \begin{cases} (\pi/2, \pi \tan(\varphi)/2), & 0 \leq \varphi \leq \pi/4, \\ (\pi \cot(\varphi)/2, \pi/2), & \pi/4 < \varphi < 3\pi/4, \\ (-\pi/2, -\pi \tan(\varphi)/2), & 3\pi/4 \leq \varphi \leq \pi. \end{cases} \quad (\text{D1})$$

The instantaneous distance between the global minima is therefore

$$d(\varphi) = \pi |\sec(\min(\varphi, |\pi/2 - \varphi|, |\pi - \varphi|))|. \quad (\text{D2})$$

The square can be parameterized into a circle with varying diameter $d(\varphi)$, the distance between the two global minima. We can therefore write an effective low-energy Hamiltonian

$$\hat{H} \approx 4E_C \hat{n}_\Theta^2 + \beta \cos[2\pi \hat{\Theta}/d(\varphi)] + 4E_C \hat{n}_\Phi^2 - \alpha \cos[d(\varphi) \hat{\Phi}/\pi], \quad (\text{D3})$$

where $\hat{\Theta} = \cos(\varphi)\hat{\theta} + \sin(\varphi)\hat{\phi}$ is defined along the radius of the rotation and $\hat{\Phi} = \cos(\varphi)\hat{\phi} - \sin(\varphi)\hat{\theta}$ is its perpendicular coordinate. To preserve the 2π periodicity of the transformed coordinates we can also renormalize $\hat{\Theta} \rightarrow d(\varphi)\hat{\Theta}/\pi$ and $\hat{\Phi} \rightarrow d(\varphi)\hat{\Phi}/\pi$. Equation (D3) gives a qualitatively good description of the adiabatic path in that it accurately follows the global minima.

Equation (D3) does not, however, capture all the low-order effects of the term $-(\zeta/2) \sin(2\varphi) \cos(\hat{\theta} - \hat{\phi})$ of Eq. (7). Beyond reducing the four-fold degeneracy to a two-fold degeneracy, this term also leads to squeezing along either $\hat{\Theta}$ or $\hat{\Phi}$ during the rotation, as observed in Fig. 3 b). This fact is better appreciated by writing $-(\zeta/2) \sin(2\varphi) \cos(\hat{\theta} - \hat{\phi})$ in terms of the rotating coordinates

$$-(\zeta/2) \sin(2\varphi) \cos(\hat{\theta} - \hat{\phi}) = -(\zeta/2) \sin(2\varphi) \cos\left([\cos(\varphi) - \sin(\varphi)] \hat{\Theta} - [\cos(\varphi) + \sin(\varphi)] \hat{\Phi}\right). \quad (\text{D4})$$

Taylor expanding Eq. (D4) to second order near $(\hat{\Theta}, \hat{\Phi}) = (0, 0)$ reveals that Eq. (D4) can be approximated with

$$-(\zeta/2) \sin(2\varphi) \cos(\hat{\theta} - \hat{\phi}) \approx (\zeta/4) \sin(2\varphi) [\cos(\varphi) - \sin(\varphi)]^2 \hat{\Theta}^2 + (\zeta/4) \sin(2\varphi) [\cos(\varphi) + \sin(\varphi)]^2 \hat{\Phi}^2. \quad (\text{D5})$$

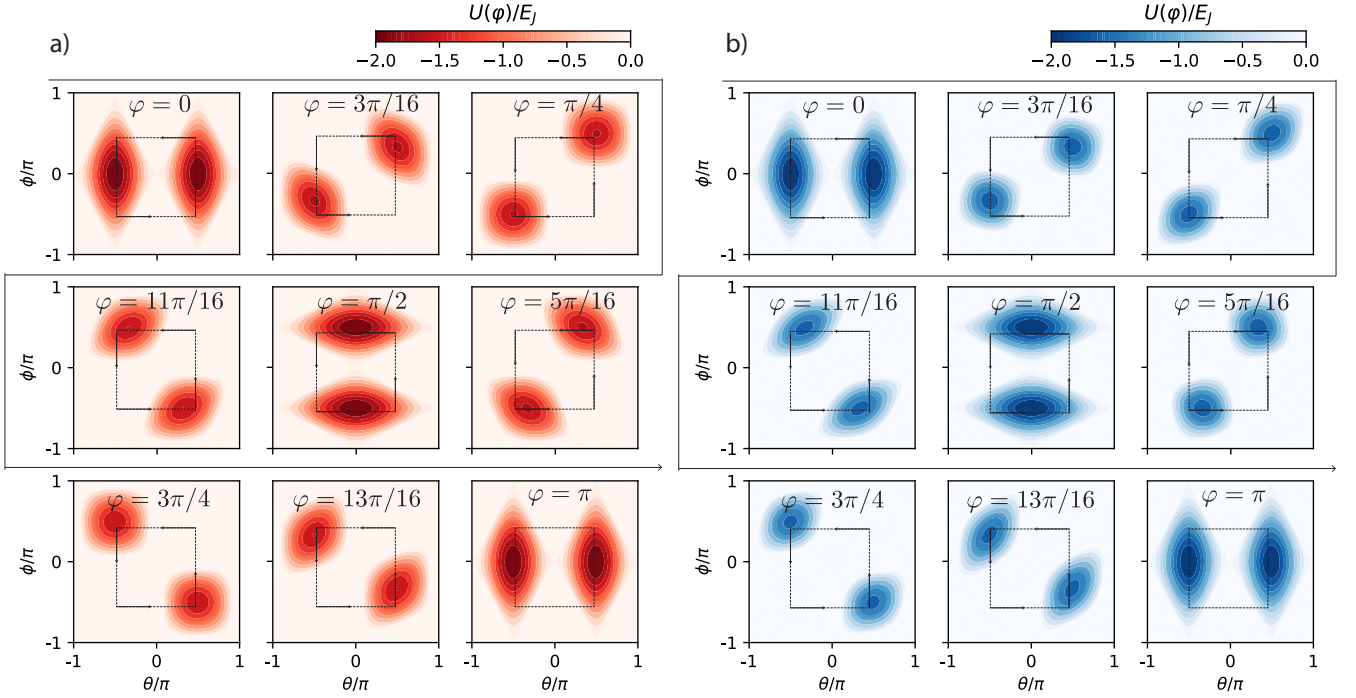


FIG. 7. a) Reproduction of Fig. 2 b) with the potential energy of the low-energy model in Eq. (D3). This low-energy model ignores the effect of the $\cos(\hat{\theta})\cos(\hat{\phi})$ term and ignores any interaction between rotating coordinates Θ and Φ which result in some additional distortion and diffusion in Fig. 2 b). b) Reproduction of Fig. 3 b) with the potential energy of Eq. (D6). This model now includes the leading order effects of the $\cos(\hat{\theta})\cos(\hat{\phi})$ term resulting in squeezing along either $\hat{\Theta}$ or $\hat{\Phi}$ and in asymmetry of the potential energy during the rotation. Any interaction between $\hat{\Theta}$ and $\hat{\Phi}$ is still ignored within the low-energy approximation.

We can therefore correct Eq. (D3) with

$$\hat{H} \approx 4E_C \hat{n}_\Theta^2 + (1 - r(\varphi))\beta \cos[2\pi\hat{\Theta}/d(\varphi)] + 4E_C \hat{n}_\Phi^2 - (1 + s(\varphi))\alpha \cos[d(\varphi)\hat{\Phi}/\pi], \quad (\text{D6})$$

where we defined

$$r(\varphi) = \frac{\zeta \sin(2\varphi)}{2\beta} \left[\frac{d(\varphi)}{2\pi} \right]^2 [\cos(\varphi) - \sin(\varphi)]^2, \quad (\text{D7})$$

$$s(\varphi) = \frac{\zeta \sin(2\varphi)}{2\alpha} \left[\frac{\pi}{d(\varphi)} \right]^2 [\cos(\varphi) + \sin(\varphi)]^2. \quad (\text{D8})$$

This distortion observed in Fig. 3 b) is however not captured by either Eq. (D3) or Eq. (D6) and results from interactions between Θ and Φ . Even though they don't significantly impact the global minima, they renormalize the matrix elements of the charge operators and cosine phase operators, as shown in Fig. 5 b-c). In particular, they become non-zero during the rotation but remain exponentially suppressed due to the disjoint support of the eigenstates.

Appendix E: Comparison of the $\sin(\theta)\sin(\phi)$ and $\cos(\theta - \phi)$ models

The ground and second excited states of both the $\sin(\theta)\sin(\phi)$ and $\cos(\theta - \phi)$ models are shown in 2D phase space in Fig. 8. These results are obtained from numerical diagonalization of the Hamiltonians in the charge basis. The conversion to phase basis is done via a Fourier transform in the two coordinates. The eigenstates are also shown in the charge basis in Fig. 9. Since the phase coordinates of the two $\cos(2\theta)$ qubits are compact the states have discrete charge states.

We remark that the low-energy eigenstates in both models share similar features. The key difference arises when comparing $\varphi = \pi/4$ and $\varphi = 3\pi/4$, especially for the second excited state. There, the states are rotated by $\pi/2$ locally

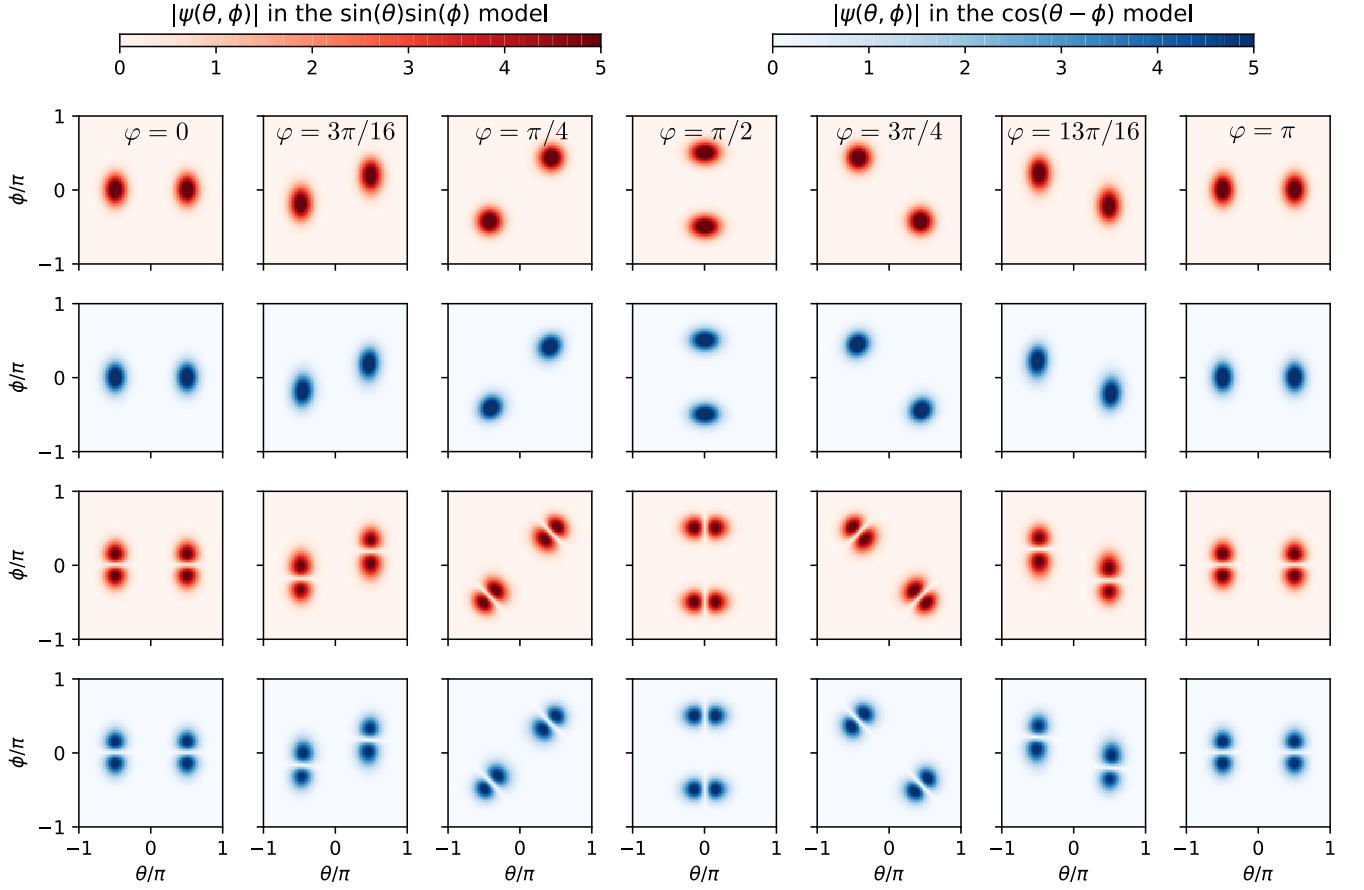


FIG. 8. Instantaneous ground state and second excited state as a function of the rotation angle φ , in phase basis, with the proposed circuit implementation in Eq. (7) (in red) and the ideal version where $\cos(\hat{\theta} - \hat{\phi}) \rightarrow \sin(\theta) \sin(\phi)$ (in blue). Here the diagonalization is realized in charge representation for both modes. The eigenstates are then Fourier transformed to return the phase representation. Here $E_C/h = 100$ MHz and $\alpha/h = \beta/h = \zeta/h = 20.0$ GHz.

near each global minimum in the 2D phase space (see Fig. 8) for $\varphi = 3\pi/4$ but not $\varphi = \pi/4$. This asymmetry results from the $\cos(\theta) \cos(\phi)$ term present in the $\cos(\theta - \phi)$ interaction. Even though this term slightly renormalizes the energies and matrix elements of the logical states, it does not prevent the formation of a double well potential at all angles φ as shown in Fig. 8. In other words, its impact on the protection of the qubit is negligible.

Appendix F: Time-dependent simulations

We promote the angle $\varphi \rightarrow \varphi(t)$ to an instantaneous angle of rotation at time t with the boundary conditions $\varphi(0) = 0$ and $\varphi(T) = \pi$ for a total gate time $t = T$.

In the spirit of Ref. [12], we introduce the time-dependent unitary $\hat{\mathcal{A}}[\varphi(t)] = \sum_n |\psi_n[\varphi(t)]\rangle \langle \psi_n(0)|$, where $|\psi_n[\varphi(t)]\rangle$ is the instantaneous eigenstates of $\hat{H}[\varphi(t)]$ with energies $\omega_n[\varphi(t)]$. The Hamiltonian can then be expressed as

$$\hat{H}_{\mathcal{A}}[\varphi(t)] = \sum_{n=0}^{\infty} \omega_n[\varphi(t)] |\psi_n(0)\rangle \langle \psi_n(0)| - i \sum_{n,m=0}^{\infty} |\psi_n(0)\rangle \left\langle \psi_n[\varphi(t)] \left| \frac{d}{dt} \right| \psi_m[\varphi(t)] \right\rangle \langle \psi_m(0)|, \quad (\text{F1})$$

where

$$\left\langle \psi_n[\varphi(t)] \left| \frac{d}{dt} \right| \psi_m[\varphi(t)] \right\rangle = \dot{\varphi} \frac{\left\langle \psi_n[\varphi(t)] \left| \frac{d\hat{H}}{d\varphi} \right| \psi_m[\varphi(t)] \right\rangle}{\omega_n[\varphi(t)] - \omega_m[\varphi(t)]} \quad (\text{F2})$$

for $\omega_n[\varphi(t)] \neq \omega_m[\varphi(t)]$.

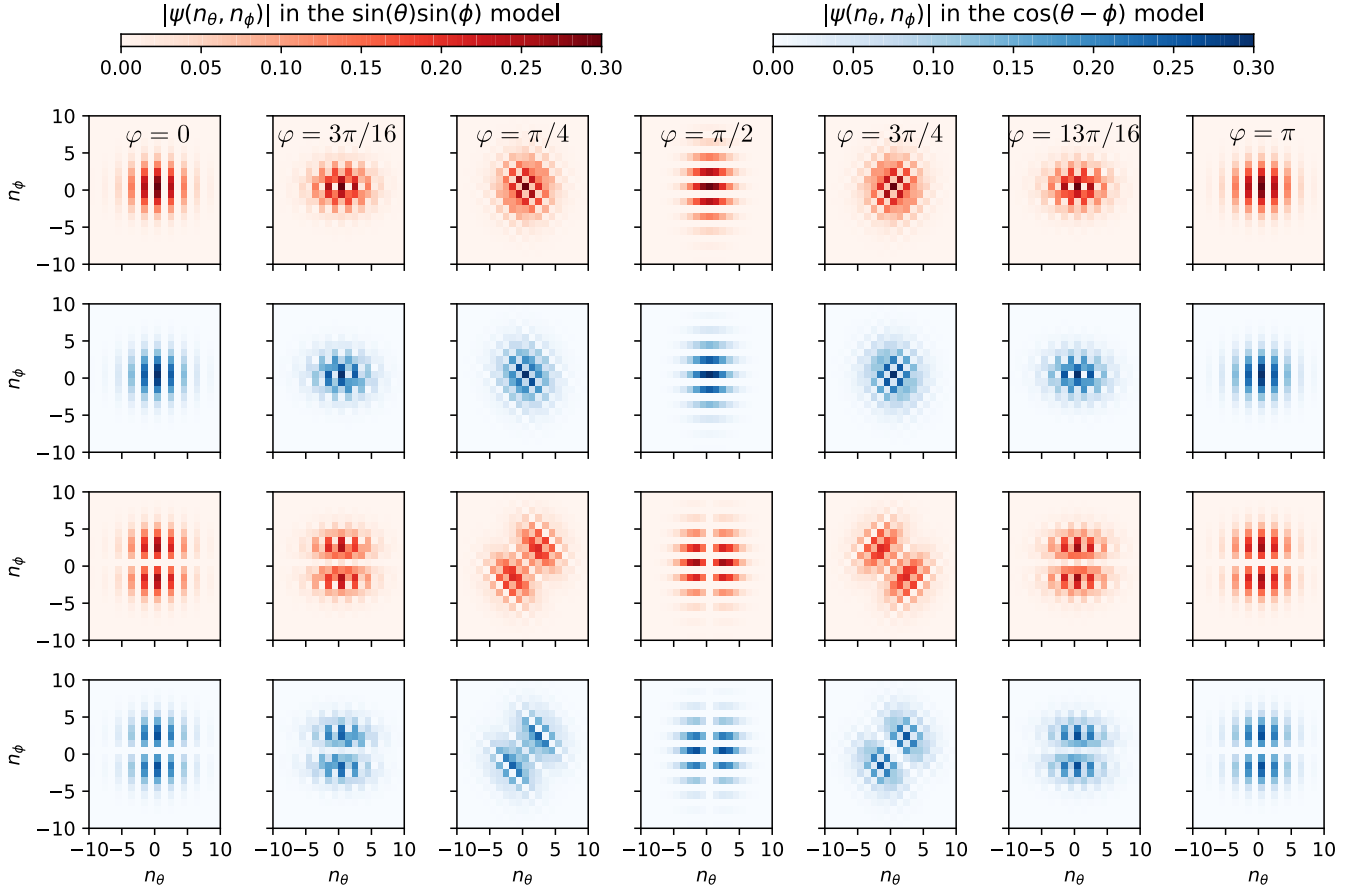


FIG. 9. Same as Fig. 8 but in the charge basis.

For the adiabatic theorem to hold, the magnitude of these matrix elements must be much smaller than $|\omega_n[\varphi(t)] - \omega_m[\varphi(t)]|$. In this case, the system remains in the n th instantaneous eigenstate. Quantum transitionless driving [12] can in principle be used to reduce the amplitude of these transitions to speed up the gate.

We optimize the shape of $\varphi(t)$ by bounding $10^{-3}|\omega_n[\varphi(t)] - \omega_m[\varphi(t)]|$ for $n = 0, 1$ at all times.

The time-dependent simulations are done in the charge basis for both compact modes θ and ϕ with sparse matrices by solving the time-dependent Schrödinger equation with the Hamiltonian in Eq. (7). The states are then converted to phase space using Fourier transforms.